Activity of Psoralen-Functionalized Nanoscintillators against Cancer Cells upon X-ray Excitation

Jonathan P. Scaffidi,[†,‡] Molly K. Gregas,[†,‡] Benoit Lauly,[†,‡] Yan Zhang,[†,‡] and Tuan Vo-Dinh[†,‡,§,*]

[†]Fitzpatrick Institute for Photonics, Duke University, Durham, North Carolina 27708, United States, [‡]Department of Biomedical Engineering, Duke University, Durham, North Carolina 27708, United States, and [§]Department of Chemistry, Duke University, Durham, North Carolina 27708, United States

ABSTRACT We report development of a nanoparticle-based, X-ray-activated anticancer "nanodrug" composed of yttrium oxide (Y_2O_3) nanoscintillators, a fragment of the HIV-1 TAT peptide, and psoralen. In this formulation, X-ray radiation is absorbed by the Y_2O_3 nanoscintillators, which then emit UVA light. Absorption of UVA photons by nanoparticle-tethered psoralen has the potential to cross-link adenine and thymine residues in DNA. UVA-induced cross-linking by free psoralen upon activation with UVA light has previously been shown to cause apoptosis *in vitro* and an immunogenic response *in vivo*. Studies using the PC-3 human prostate cancer cell line demonstrate that X-ray excitation of these psoralen-functionalized Y_2O_3 nanoscintillators yields concentration-dependent reductions in cell number when compared to control cultures containing psoralen-free Y_2O_3 nanoscintillators.

KEYWORDS: PUVA · psoralen · nanoscintillator · yttrium oxide · Y_2O_3

More than a million individuals in the United States are diagnosed with cancer each year, and annual cancer diagnoses worldwide number above 10 millon. Traditional approaches such as surgery, chemotherapy, radiation therapy, photodynamic therapy (PDT), and psoralen + UVA (PUVA) have shown great success in treating various types of cancer, but many additional lives could be saved through development of more effective, more universally applicable, less invasive means of therapy. To that end, the rapidly developing field of nanomedicine has attempted to leverage the untapped potential of nanomaterials as a means of improving drug targeting to and uptake by tumors, locally activating therapeutic agents, and limiting side-effects that may negatively impact patients' quality of life.[1−4]

These attempts to develop nanoparticulate anticancer drugs typically take one of three approaches. In the first, nanoparticles are used to aid in transport and delivery of chemotherapeutic agents.[5−8] Such a methodology has shown some potential, particularly in reducing the negative side-effects of chemotherapy.[9] In a second approach, the nanoparticles themselves have been used as a means of enhancing the normal effects of some, more traditional treatment.[8,10−15] Two promising techniques that fall into this category are induction of hyperthermia when illuminating gold nanoshells with infrared light[13,14] and enhancement of reactive oxygen species (ROS) generation using gold nanomaterials and X-ray radiation.[12,16−18] A third, less-proven application of nanomaterials in cancer therapy is a combination of ROS-generating PDT drugs and nanoparticles that emit UV or visible light through downconversion of X-ray radiation or upconversion of IR light.[19−27] Of these three approaches, the use of tissue-penetrating X-rays in the third case is perhaps the most intriguing. Ideally, treatment using a combination of targeted drug delivery and localized X-ray activation could be used to kill only those cells that both took up the nanodrug and were exposed to X-ray radiation. As a result, the negative side-effects associated with nonspecific uptake of chemotherapeutic drugs should be greatly reduced. At the same time, radiation doses could potentially be reduced to the point where the systemic effects associated with traditional radiation therapy (*e.g.*, nausea, fatigue) becomes relatively minor or nonexistent. Unfortunately, while such an approach with traditional PDT drugs has potential in well-oxygenated tissue, reduced ROS generation in the hypoxic environments[28−31] associated with many tumors is likely to limit the broader utility of ROS-dependent locally activated therapies. In an effort to circumvent the limitations inherent to oxygenation-dependent approaches and to take advantage of psoralen's demonstrated immunogenic potential,[32−34] we have recently pursued development of anticancer drugs in which scintillating nanoparticles ("nanoscintillators") can be used to activate psoralen in deep tissue. Having

* Address correspondence to tuan.vodinh@duke.edu.

Received for review February 8, 2011 and accepted May 9, 2011.

Published online May 09, 2011
10.1021/nn200511m

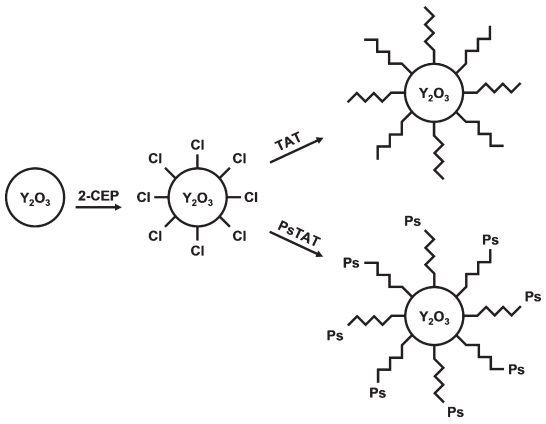

Scheme 1. Attachment of TAT and PsTAT to Y_2O_3 nanoscintillators.

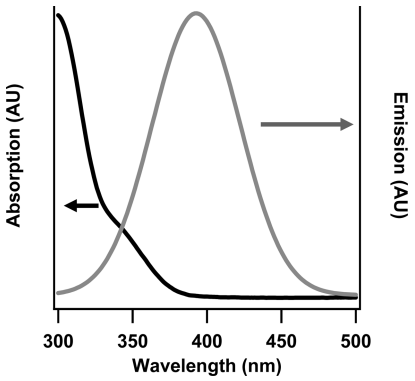

Figure 1. Absorption of psoralen and scintillation by Y_2O_3. The X-ray-excited scintillation spectrum of Y_2O_3 nanoparticles (gray trace) partially overlaps the absorption spectrum of psoralen (black trace). Spectral overlap between 320 and 405 nm has the potential to produce psoralen-DNA monoadducts and diadducts (cross-links).

previously observed no visually or statistically significant indication of psoralen activation when exposing cell cultures simultaneously co-incubated with 8-methoxypsoralen and psoralen-free nanoscintillators to X-ray radiation, we instead turned to the use of psoralen that has been physically attached to nanoscintillators. In the most effective drug−nanoscintillator configuration we have tested to date, psoralen is bound to a fragment of the HIV-1 TAT cell-penetrating/nuclear targeting peptide anchored to UVA-emitting Y_2O_3 nanoscintillators (Scheme 1).

Experiments performed with this particular nanodrug formulation over the course of several months indicate that it is nontoxic to PC-3 human prostate cancer cells at concentrations approaching 30 μg/mL in the absence of X-ray radiation. Approximately one week after X-ray exposure, however, the cell number of cultures incubated with Y_2O_3 nanoscintillators functionalized with the HIV-1 TAT fragment but lacking psoralen (hereafter referred to as "TAT-Y_2O_3") is 75 $\pm$ 8.3% (one standard deviation, number of replicates "*n*" = 26) that of cultures exposed to an equal dose of X-ray radiation in the absence of Y_2O_3 nanoscintillators. When compared to these same control cultures lacking Y_2O_3, the cell number for PC-3 cultures exposed to X-ray radiation following incubation with Y_2O_3 nanoscintillators functionalized with the HIV-1 TAT fragment with a single psoralen molecule bound to its N-terminus (hereafter referred to as "PsTAT-Y_2O_3") is reduced to 66 $\pm$ 8.1% (one standard deviation, number of replicates "*n*" = 26). When these results are normalized against the cell number of cultures irradiated after incubation with TAT-Y_2O_3 to correct for the well-established ability of hard matter to amplify the antitumor effects of X-ray radiation, the relatively modest 9% absolute difference in cell number increases somewhat to 12%. These differences in relative cell number are statistically distinguishable at Y_2O_3 concentrations from ~9.5 to ~95 μg/mL, as determined by *t*-tests, and show clear concentration dependence. These results represent the first evidence of drug-associated, X-ray-activated reductions in cell growth for psoralen tethered to scintillating nanomaterials. The anticancer immunogenic potential of this and future formulations, of course, can be fully evaluated only *in vivo*.

APPROACH

As with more traditional light-activated therapies, the X-ray-excited nanoscintillator emission spectrum must at least partially overlap the psoralen absorption spectrum, as shown in Figure 1. This fundamental requirement indicates that many or most currently available scintillators will be inappropriate for psoralen activation (in large part because they have generally been developed for use with silicon-based photodetectors, which are most sensitive in the green and red portions of the visible spectrum rather than the UV). The range of suitable materials for *in vitro* and *in vivo* use is further limited by the necessity that the nanoscintillators be insoluble in water, as solid-state scintillators lose their emissive properties upon dissolution. Lack of toxicity is also desirable, but is not necessarily critical if the nanoscintillators are demonstrably less hazardous than the disease to be treated. Both concerns can potentially be addressed if the nanoscintillators can be covered with some optically transparent coating (*e.g.*, SiO_2) that is impermeable to water and toxins.

Table 1 lists a small subset of the UVA-emitting scintillators that can potentially activate DNA monoadduct or diadduct formation (*e.g.*, cross-linking) by psoralen.[35−59] Several of these materials such as cubic-phase Y_2O_3, a scintillator whose emission is due to recombination of self-trapped excitons at defect sites within the bulk matrix,[56] are commercially available as nanoscintillators or can be readily synthesized in the laboratory using published methods.[60−64] Others, such as the cerium-doped perovskites $YAlO_3$:Ce and $LuAlO_3$:Ce, whose scintillation is associated with energy transfer from the bulk matrix to the cerium dopant,[65−67] are

TABLE 1. UVA-Emitting Scintillating Nanoparticles[a]

material	λ_{max} (nm)	photons per MeV at 662 keV	limitation	ref
$CeBr_3$	371	68 000	WS	35
$CeCl_3$	350	46 000	WS	36
$GdAlO_3$:Ce	335–360	9000	NCN	37
K_2CeCl_5:Ce	370	30 000	WS	38
K_2LaBr_5:Ce	355–390	40 000	WS	39
K_2LaCl_5:Ce	340–375	39 650	WS	39, 40
K_2LaI_5:Ce	340–380	29 000	WS	39, 41
KYP_2O_7:Ce	380	10 000	NCN	42
$LaBr_3$:Ce	355–390	67 500	WS	43–46
$LaCl_3$:Ce	330–355	49 000	WS	43, 45, 46
$LuAlO_3$:Ce	365	16 350	NCN	47–50
$LuPO_4$:Ce	360	17 200	NCN	51
$PbSO_4$	340–380	10 000	TX	52–54
$PrBr_3$:Ce	365–395	21 000	NCN, WS	55
Y_2O_3	370	15 480		56
$YAlO_3$:Ce	345–365	18 360	NCN	49, 50, 57–59

[a] Light yield (photons per MeV of absorbed X-ray radiation) at 662 keV describes how efficiently each material converts X-ray photons into UVA photons; WS = water-soluble; NCN = no commercially available nanoparticles; TX = toxic.

less immediately available as nanoparticles but may be superior psoralen activation sources due to their emission wavelengths and the efficiency with which they downconvert X-ray photons to UVA photons.

In these particular studies, we have used commercially available ~12 nm diameter cubic-phase Y_2O_3 nanoscintillators functionalized with a psoralen-containing, thiol-modified fragment of the HIV-1 TAT peptide ("PsTAT-Y_2O_3", peptide sequence psoralen-Arg-Lys-Lys-Arg-Arg-Arg-Gln-Arg-Arg-Cys-$CONH_2$). Our own prior research[68] and that of various other researchers[69–71] have shown that this peptide sequence can improve the uptake, intracellular transport, and nuclear localization of biomolecules and nanoparticles. A similar peptide of identical amino acid sequence but lacking psoralen was attached to Y_2O_3 nanoscintillators ("TAT-Y_2O_3") for use as a control when determining the extent to which intrinsic X-ray–Y_2O_3 interactions and particle adhesion to the cell culture plates affected cell number. Both Y_2O_3[72,73] and this particular segment of the HIV-1 TAT sequence[74–76] have been shown to be nontoxic in the absence of X-ray exposure, thereby making this nanodrug formulation a first-generation candidate for further proof-of-concept studies. Further research and development with more strongly emitting nanoscintillators and the increasing variety of cell penetrating/nuclear targeting peptides are likely to yield more active nanodrug candidates.

RESULTS AND DISCUSSION

Like clonogenics,[77–79] trypan blue staining,[77,80] or mitochondrial activity assays,[80] cell number measurement cannot in and of itself identify the biochemical pathway or pathways by which a drug candidate acts. Careful experimental design, however, does allow

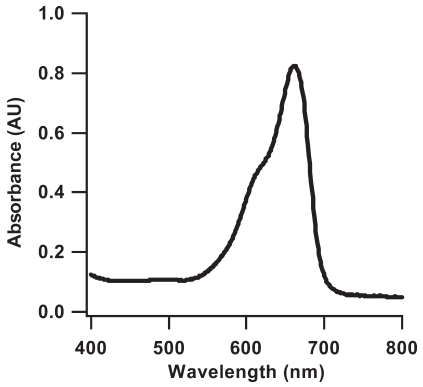

Figure 2. Visible-wavelength methylene blue absorption spectrum. The relative visible-wavelength absorption of methylene blue at ~660 nm following desorption from cell culture with acidified ethanol is an accepted indicator of cell number density.

determination of the extent to which the presence of a psoralen moiety at the N-terminus of the PsTAT peptide affects the proliferation of cell cultures incubated with PsTAT-Y_2O_3 *versus* cell cultures incubated with equivalent concentrations of TAT-Y_2O_3. Logically, any relative increase or decrease in cell number for PC-3 cell cultures exposed to the PsTAT-functionalized nanodrug in the presence or absence of X-ray exposure must be attributed to the presence of the N-terminal psoralen moiety. Further, any differences in the PsTAT-Y_2O_3/TAT-Y_2O_3 cell number ratio in the presence *versus* the absence of irradiation can reasonably be attributed to interactions between PsTAT-Y_2O_3 and X-ray radiation, although the specific nature of those interactions cannot be determined on the basis of cell number measurements.

Figure 2 shows a representative visible-wavelength methylene blue absorption spectrum following desorption from cells using 1:1 (v/v) ethanol/0.1 M HCl. The absorption profile matches that published by prior users of this assay, confirming the lack of dimer formation.[81–86] Using the absorption intensity at ~660 nm, this assay has been shown to allow reliable quantitative determination of cell number in a variety of plating formats.[83]

Figure 3a shows visible-wavelength methylene blue absorption results at ~660 nm for cultures with and without TAT-Y_2O_3 (squares) or PsTAT-Y_2O_3 (diamonds) in the absence of X-ray exposure. The data have been normalized against the particle-free controls incorporated into each six-well plate, allowing correction for minor plate-to-plate variability in the cell seeding density, the quality of the cell culture coating, plate-to-plate temperature variations during handling, *etc.* A decrease in the normalized cell number relative to particle-free controls is apparent at a PsTAT-Y_2O_3 concentration of 95 μg/mL, but no visually or statistically significant difference is apparent at lower concentrations of either TAT- or PsTAT-functionalized nanoscintillators in the

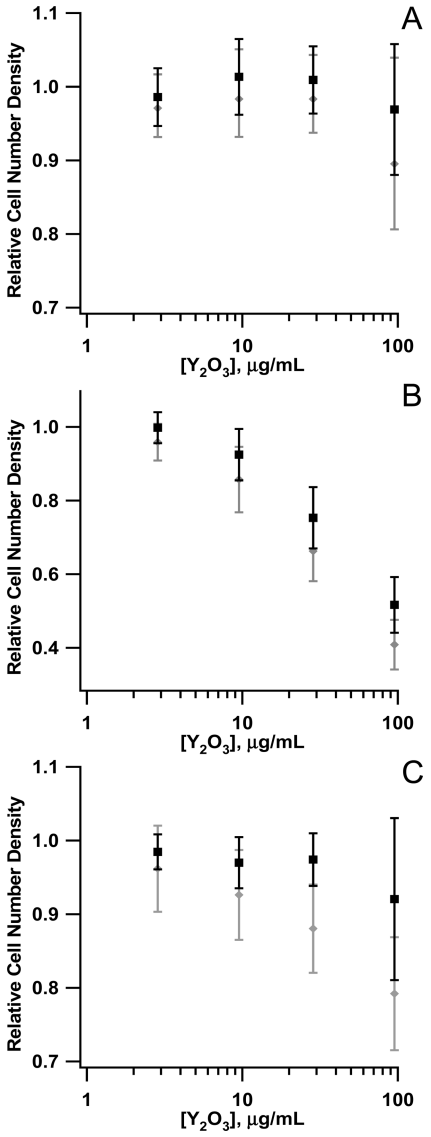

Figure 3. Normalized cell number density of PC-3 human prostate cancer cell cultures treated with TAT-Y_2O_3 or PsTAT-Y_2O_3 with and without X-ray exposure. (A) Control-normalized relative cell number of cultures incubated with TAT-Y_2O_3 (black squares) or PsTAT-Y_2O_3 (gray diamonds), but not exposed to X-ray radiation. (B) As in (A), but approximately one week after X-ray irradiation. (C) Relative cell number of cultures incubated to PsTAT-Y_2O_3 *versus* TAT-Y_2O_3 with (gray diamonds) and without (black squares) of X-ray exposure. Y_2O_3 concentrations are defined as the concentration in culture, and error bars represent one standard deviation.

absence of X-ray irradiation. As expected based on the demonstrated lack of toxicity for Y_2O_3[72,73] and this portion of the TAT peptide,[74−76] these results confirm the lack of strong intrinsic toxicity for TAT-Y_2O_3 and PsTAT-Y_2O_3 in the absence of X-ray irradiation.

This picture changes substantially upon addition of X-ray radiation. Figure 3b shows cell number results for PC-3 cell cultures incubated with TAT-Y_2O_3 (squares) or PsTAT-Y_2O_3 (diamonds) at particle concentrations ranging from 2.9 to 95 μg/mL prior to irradiation. As in Figure 3a, the data have been normalized against in-plate controls lacking either of the nanoscintillator formulations. In addition to correcting for minor plate-to-plate variability in cell seeding, plate handling, *etc.*, this normalization additionally allows straightforward correction for the established ability of X-ray radiation to directly impact cell viability and propagation, such as is intentionally used when treating cancer with radiotherapy.

As can be seen in Figure 3b, X-ray exposure following incubation with either TAT-Y_2O_3 or PsTAT-Y_2O_3 reduces cell number in a particle dose-dependent manner at Y_2O_3 concentrations between 9.5 and 95 μg/mL when compared to irradiated particle-free control cultures. Specifically, X-ray irradiation of PC-3 cell cultures incubated with 2.9−95 μg/mL TAT-functionalized Y_2O_3 reduces the normalized cell number from 1.00 $\pm$ 0.042 (one standard deviation) at 2.9 μg/mL Y_2O_3 to 0.98 $\pm$ 0.070 at 9.5 μg/mL, 0.75 $\pm$ 0.083 at 29 μg/mL, and 0.52 $\pm$ 0.076 at 95 μg/mL Y_2O_3. For cultures incubated with PsTAT-functionalized Y_2O_3 prior to irradiation, the normalized cell number decreases from 0.96 $\pm$ 0.050 at 2.9 μg/mL Y_2O_3 to 0.86 $\pm$ 0.089 at 9.5 μg/mL, 0.66 $\pm$ 0.082 at 29 μg/mL, and 0.41 $\pm$ 0.067 at 95 μg/mL Y_2O_3. The general trend of reduced cell number densities at elevated particle concentrations is not unexpected, as X-ray interaction with hard matter is known to enhance the effectiveness of radiotherapy independent of PDT or PUVA effects.[20,25,87,88] Interestingly, however, the cell number of cultures incubated with PsTAT-Y_2O_3 is universally lower than that of PC-3 cell cultures incubated with an equal concentration of TAT-Y_2O_3 prior to X-ray irradiation. This distinction is not evident at the lowest particle concentration tested, but at TAT-Y_2O_3 and PsTAT-Y_2O_3 concentrations greater than or equal to ~9.5 μg/mL differentiation between cultures incubated with TAT-Y_2O_3 *versus* PsTAT-Y_2O_3 prior to X-ray exposure is both visually and statistically apparent (Figure 3b and Table 2).

These differences in cell number become more evident after correction for the intrinsic X-ray−hard matter interactions, which have been utilized so effectively in radiation therapy.[89−92] To that end, Figure 3c displays the renormalized cell number of PC-3 cultures incubated with PsTAT-Y_2O_3 *versus* TAT-Y_2O_3 with (squares) and without (diamonds) X-ray irradiation. The value of 0.98 $\pm$ 0.024 at 2.9 μg/mL in the absence of X-ray exposure, for example, confirms that the cell number of PC-3 cultures exposed to 2.9 μg/mL PsTAT-Y_2O_3 is approximately equal to that of cultures exposed to 2.9 μg/mL TAT-Y_2O_3 in the absence of irradiation. As noted above, this baseline cell number remains stable in the absence of irradiation up to particle concentrations of 95 μg/mL in the absence of X-ray exposure, at which point the cell number of cultures incubated with PsTAT-Y_2O_3 falls to 0.92 $\pm$ 0.110 *versus* that of cultures incubated with TAT-Y_2O_3. The cause for this decrease in cell number at high particle concentration in the absence of X-ray radiation is not yet clear, but will be a subject of future studies.

TABLE 2. Normalized Cell Number (#) of PC-3 Human Prostate Cancer Cell Cultures Treated with TAT-Y_2O_3 or PsTAT-Y_2O_3 in the Presence and Absence of X-ray Irradiation[a]

formulation	Y_2O_3 concentration (μg/mL)	± X-ray	*N*	cell # vs Y_2O_3-free control			*p vs* Y_2O_3-free control	cell # *vs* TAT-Y_2O_3			*p vs* TAT-Y_2O_3
TAT-Y_2O_3	95	–	20	0.97	±	0.089	0.21				
	29	–	14	1.01	±	0.046	0.36				
	9.5	–	21	1.01	±	0.051	0.39				
	2.9	–	15	0.99	±	0.039	0.21				
PsTAT-Y_2O_3	95	–	20	0.90	±	0.144	0.013	0.92	±	0.110	0.030
	29	–	14	0.98	±	0.0360	0.19	0.97	±	0.036	0.10
	9.5	–	21	0.98	±	0.068	0.32	0.97	±	0.035	0.056
	2.9	–	15	0.97	±	0.046	0.058	0.98	±	0.024	0.17
TAT-Y_2O_3	95	+	33	0.52	±	0.076	$<1 \times 10^{-4}$				
	29	+	26	0.75	±	0.083	$<1 \times 10^{-4}$				
	9.5	+	33	0.92	±	0.070	0.043				
	2.9	+	28	1.00	±	0.042	0.46				
PsTAT-Y_2O_3	95	+	33	0.41	±	0.067	$<1 \times 10^{-4}$	0.79	±	0.077	$<1 \times 10^{-4}$
	29	+	26	0.66	±	0.082	$<1 \times 10^{-4}$	0.88	±	0.060	1.2×10^{-4}
	9.5	+	33	0.86	±	0.089	1.3×10^{-3}	0.93	±	0.061	5.3×10^{-4}
	2.9	+	28	0.96	±	0.140	0.14	0.96	±	0.058	1.2×10^{-3}

[a] Y_2O_3 concentration = TAT-Y_2O_3 and PsTAT-Y_2O_3 concentrations in culture; *N* = total number of replicates; cell # vs Y_2O_3-free control = cell # of cultures exposed to TAT-Y_2O_3 or PsTAT-Y_2O_3, normalized against in-plate controls lacking either of the nanodrugs but exposed to a matching dose of X-ray radiation; *p* = *p* value determined using a one-tailed, unpaired *t*-test; cell # *vs* TAT-Y_2O_3 = cell # of cultures exposed to PsTAT-Y_2O_3, normalized against in-plate controls exposed to a matching dose of X-ray radiation.

For irradiated *versus* nonirradiated PC-3 cell cultures, the normalized data in Figure 3c indicate that there is no obvious PsTAT-Y_2O_3 *versus* TAT-Y_2O_3 effect at a Y_2O_3 concentration of 2.9 μg/mL. A clear, visually and statistically significant downward trend in the relative cell number ratio is observable for irradiated cell cultures at PsTAT-Y_2O_3 concentrations from 9.5 to 95 μg/mL. Specifically, the cell number ratio for PC-3 cultures irradiated after incubation with PsTAT-Y_2O_3 *versus* TAT-Y_2O_3 falls from 0.96 ± 0.058 (one standard deviation) at 2.9 μg Y_2O_3 per mL to 0.93 ± 0.061 at 9.5 μg/mL, 0.88 ± 0.060 at 29 μg/mL and 0.79 ± 0.077 at PsTAT-Y_2O_3 and TAT-Y_2O_3 concentrations of 95 μg/mL. The number of replicates ("*n*") at each concentration and the *p* values for differentiation of the PsTAT-Y_2O_3:TAT-Y_2O_3 cell number ratio in the presence or absence of X-ray exposure as determined using an unpaired, one-tailed *t*-test are listed in Table 3. Although the calculated *p* value at the lowest tested concentration of PsTAT- and TAT-Y_2O_3 provides little suggestion that psoralen activation upon irradiation significantly affects PC-3 cell growth or viability at this particle concentration, statistically significant differences in the PsTAT-Y_2O_3:TAT-Y_2O_3 cell number ratio become evident at higher Y_2O_3 concentrations. At 9.5 μg/mL Y_2O_3, for example, the probability of a false positive result for irradiated *versus* unirradiated cultures falls below 1%, as evaluated by an unpaired one-tailed *t*-test. The likelihood of a false positive result decreases yet further as the concentrations of PsTAT-Y_2O_3 and TAT-Y_2O_3 are increased, falling below 10^{-4} (*e.g.*, 0.01%) at Y_2O_3 concentrations above 29 μg/mL.

TABLE 3. Normalized Cell Number (#) of PC-3 Human Prostate Cancer Cell Cultures Treated with PsTAT-Y_2O_3 in the Presence and Absence of X-ray Irradiation[a]

Y_2O_3 concentration (μg/mL)	± X-ray	*N*	PsTAT-Y_2O_3/TAT-Y_2O_3 cell # ratio			*p vs* un irradiated cell cultures
95	–	20	0.92	±	0.110	
29	–	14	0.97	±	0.036	
9.5	–	21	0.97	±	0.035	
2.9	–	15	0.98	±	0.024	
95	+	33	0.79	±	0.077	$<1 \times 10^{-4}$
29	+	26	0.88	±	0.060	$<1 \times 10^{-4}$
9.5	+	33	0.93	±	0.060	7.4×10^{-4}
2.9	+	28	0.96	±	0.058	0.039

[a] Y_2O_3 concentration = TAT-Y_2O_3 and PsTAT-Y_2O_3 concentrations in culture; *N* = total number of replicates; PsTAT-Y_2O_3/TAT-Y_2O_3; cell # ratio = cell # of cultures exposed to PsTAT-Y_2O_3, normalized against in-plate controls incubated with a matching concentration of TAT-Y_2O_3 and exposed to a matching dose of X-ray radiation; *p* = *p* value determined using a one-tailed, unpaired *t*-test.

The broader anticancer potential of the *in vitro* results detailed above is not yet clear and cannot be evaluated in the absence of an intact, functional immune system because the underlying hope in coupling psoralen to UVA-emitting nanoscintillators is to activate psoralen's demonstrated immunogenic properties by exposing deep-seated tumors to both the nanodrug and X-ray radiation. Such studies are planned, as are *in vitro* experiments examining the effectiveness of PsTAT-Y_2O_3 against other cell lines. Similarly, investigations attempting to determine the

mechanism by which PsTAT-Y_2O_3 either kills or delays the growth of PC-3 human prostate cancer cells are ongoing.

CONCLUSIONS

Although the *in vitro* reductions in cell number observed in the current study are modest, they provide the first ever demonstration of cell killing or growth inhibition by X-ray excited, psoralen-functionalized nanoscintillators. Specifically, these cell number results provide preliminary evidence that X-ray exposure of Y_2O_3 nanoparticles functionalized with a psoralen-modified nuclear targeting peptide may have potential in the fight against cancer. If psoralen continues to act *via* a non-ROS-dependent mechanism after attachment to these nanoscintillators, then such a drug−peptide−particle nanoconjugate may have unique potential as a means of treating deep-seated tumors in hypoxic environments. Further research is underway to determine the mechanism of action for these particular psoralen-functionalized nanoscintillators and to better quantify their ability to inhibit cell growth and/or induce apoptosis. At the same time, we are examining the *in vitro* potential of other UV-emitting nanoscintillators such as doped oxides, fluorides, and perovskites; cell-penetrating/nuclear-targeting peptides such as penetratin, MAP, polyarginine, c-Fos, Antennapedia, VP22, and transportan; and the *in vitro* effectiveness of nanoscintillators functionalized with a combination of psoralen-modified and psoralen-free cell-penetrating/nuclear-targeting peptides. The results of these studies will be the focus of future reports.

EXPERIMENTAL SECTION

Nanodrug Preparation. During the synthesis of the unoptimized nanodrug, commercially available ~12 nm diameter cubic-phase Y_2O_3 nanoscintillators (Meliorum Technologies, Rochester, NY) were weighed, autoclaved, and dispersed using tip sonication at 1 mg/mL in sterile-filtered 5 mg/mL 2-chloroethyl phosphonic acid ("2-CEP", Fisher Scientific, Fairlawn, NJ) dissolved in 100 mM pH ~7 sodium bicarbonate (VWR, West Chester, PA) prepared using sterile water for injection ("SWFI", EMD Chemicals, Gibbstown, NJ). The dispersed nanoscintillators were then vigorously mixed for 48 h at room temperature to allow 2-CEP attachment and purified by triplicate centrifugation at ~15 500 RCF for 30 min (centrifuge model 5804, Eppendorf, New York, NY). Following the third centrifugation, the particles were redispersed in sterile-filtered TAT (SynBioSci, Livermore, CA) or PsTAT solution (RS Synthesis LLC, Lexington, KY) prepared at 1 mg/mL in pH ~6.5 SWFI. The nanoscintillators were again vigorously mixed for 48 h at room temperature to allow attachment of the TAT or PsTAT peptide to the surface-associated 2-CEP *via* thioether formation. Afterward, the peptide−nanoscintillator conjugates were again purified by triplicate centrifugation, with final redispersion by brief tip sonication in sterile-filtered 5 wt % dextrose ("D5W", Mallinckrodt Baker Inc., Phillipsburg, NJ) prepared with SWFI.

These TAT-Y_2O_3 and PsTAT-Y_2O_3 formulations were typically added to cell culture within ~3 h of preparation and were briefly tip-sonicated immediately before addition to cultures to mitigate the potential effects of aggregation during storage.

***In Vitro* Nanodrug Testing.** During *in vitro* testing, PC-3 human prostate cancer cells (American Type Culture Collection, Rockville, MD) were grown to ~70% confluence in F12-K cell culture media (Gibco, Grand Island, NY) supplemented with 10% fetal bovine serum ("FBS", Gibco, Grand Island, NY), harvested by trypsinization (Gibco, Grand Island, NY), and seeded in six-well cell culture plates (Corning, Lowell, MA) at 10^4 cells per well, in 2 mL of F12-K media supplemented with 10% FBS. The cells were allowed ~24 h to attach; then 100 μL of D5W, D5W containing TAT-Y_2O_3, or D5W containing PsTAT-Y_2O_3 was added to each well and distributed by orthogonal mixing, increasing the total media volume per well to 2.1 mL. After incubation for 3−4 h under standard conditions to allow nanoscintillator uptake and intracellular transport, test cultures were exposed to 2 Gy X-ray radiation at 160 or 320 kVp, with the dose hardened using a 2 mm Al filter (model: X-RAD 320, Precision X-ray Inc., North Branford, CT). Control cultures were treated with D5W, D5W containing TAT-Y_2O_3, or D5W containing PsTAT-Y_2O_3 but were not irradiated. The culture media was removed from all plates by aspiration immediately after X-ray exposure of the test plates and replaced with 2 mL of F12-K supplemented with 10% FBS. The PC-3 cell cultures were then incubated under standard conditions for 7−8 days prior to cell number determination.

TAT-Y_2O_3 and PsTAT-Y_2O_3 nanodrug concentrations were confirmed by inductively coupled plasma atomic emission spectrometry (ICP-AES) determination of yttrium content. After the six centrifugations performed during preparation, Y_2O_3 concentrations were typically within ~5% of the expected concentration. No systematic error in the Y_2O_3 concentration was observed for either TAT-Y_2O_3 or PsTAT-Y_2O_3. Because TAT and PsTAT are tethered to the Y_2O_3 nanoscintillators, we presume that the TAT and PsTAT concentrations also vary to a similar extent. We have attempted to quantify the amount of peptide attached to the Y_2O_3 nanoscintillators by various techniques (UV−visible absorption spectroscopy, fluorescence, MALDI, LC-MS, *etc.*) and have repeatedly found that the amount of peptide in the nanodrug formulation is below the limit of detection for most of these techniques when applied to Y_2O_3-containing samples. The exception is fluorescence, with which we have detected a weak but recognizable psoralen spectrum in the PsTAT-Y_2O_3 formulation. The intrinsic difficulties of quantifying particle-tethered fluorophores (*e.g.*, hyper/hypochromism, energy transfer to/from the particle surface, path-length effects due to scattering) unfortunately prevent a quantitative determination of the nanoscintillator-tethered psoralen concentration at this time. One area of focus during future studies, however, will be the development of improved analytical methods and protocols that are better able to quantify all components of this and other nanodrugs. Extended discussion of these ongoing efforts is beyond the scope of this article and will be the subject of a future report.

Determination of Relative Cell Proliferation. After incubation under standard conditions for 7−8 days, the cell culture media was removed by aspiration and replaced with 1 mL of 0.5% (w/v) methylene blue hydrate (Sigma-Aldrich, Milwaukee, WI) in 50:50 (v/v) methanol/water. The cells were simultaneously fixed and stained for 10 min, after which the methylene blue solution was poured off and the six-well plates were gently rinsed three times with DI water. Upon drying in air for >48 h, 1 mL of 50:50 (v/v) ethanol/0.1 M HCl was added to each well and the six-well plates were gently fully homogenized on a laboratory shaker for 10 min to ensure full dye desorption from the entirety of each well. Finally, the UV−visible absorption spectrum was measured from 400 to 800 nm using a plate reader (model: Fluostar Omega, BMG Labtech, Cary, NC), and the absorption at ~660 nm was used to determine relative cell number densities. Use of in-plate particle-free and TAT-Y_2O_3 controls allows for

improved determination of nanodrug effectiveness as compared to studies that cannot correct for plate-to-plate variability in cell seeding, cell survival due to minor variations in handling, minor differences in the duration of staining, *etc*. In addition, use of acidified ethanol appears to dissolve any incidental amounts of residual Y_2O_3 that may remain in the six-well culture plates following media exchange, aspiration, methylene blue staining, and triplicate rinsing with DI water, as we have noted no increase in apparent absorption during control experiments lacking methylene blue. This is perhaps unsurprising given the small amount of Y_2O_3 present after so many rinses, the pH of the dye desorption solution (~1.3), and the ease with which Y_2O_3 dissolves in such acidic, HCl-containing solutions.

Data Manipulation. All calculations (*e.g.*, normalization, *t*-tests) were performed using Microsoft Excel 2003, SP3 (Microsoft, Redmond, OR).

Acknowledgment. The authors gratefully acknowledge many productive discussions with Dr. Guy Griffin and financial support from Immunolight, LLC.

REFERENCES AND NOTES

1. Brigger, I.; Dubernet, C.; Couvreur, P. Nanoparticles in Cancer Therapy and Diagnosis. *Adv. Drug Delivery Rev.* **2002**, *54*, 631–651.
2. Yih, T. C.; Wei, C. Nanomedicine in Cancer Treatment. *Nanomedicine (N. Y., NY, U. S.)* **2005**, *1*, 191–192.
3. Cuenca, A. G.; Jiang, H. B.; Hochwald, S. N.; Delano, M.; Cance, W. G.; Grobmyer, S. R. Emerging Implications of Nanotechnology on Cancer Diagnostics and Therapeutics. *Cancer* **2006**, *107*, 459–466.
4. Huang, X.; Jain, P. K.; El-Sayed, I. H.; El-Sayed, M. A. Gold Nanoparticles: Interesting Optical Properties and Recent Applications in Cancer Diagnostics and Therapy. *Nanomedicine (N. Y., NY, U. S.)* **2007**, *2*, 681–693.
5. Gulyaev, A. E.; Gelperina, S. E.; Skidan, I. N.; Antropov, A. S.; Kivman, G. Y.; Kreuter, J. Significant Transport of Doxorubicin into the Brain with Polysorbate 80-Coated Nanoparticles. *Pharm. Res.* **1999**, *16*, 1564–1569.
6. Song, M.; Wang, X. M.; Li, J. Y.; Zhang, R. Y.; Chen, B. A.; Fu, D. G. Effect of Surface Chemistry Modification of Functional Gold Nanoparticles on the Drug Accumulation of Cancer Cells. *J. Biomed. Mater. Res., Part A* **2008**, *86A*, 942–946.
7. Nystrom, A. M.; Xu, Z. Q.; Xu, J. Q.; Taylor, S.; Nittis, T.; Stewart, S. A.; Leonard, J.; Wooley, K. L. SCKs as Nanoparticle Carriers of Doxorubicin: Investigation of Core Composition on the Loading, Release and Cytotoxicity Profiles. *Chem. Commun.* **2008**, 3579–3581.
8. Rapoport, N.; Gao, Z. G.; Kennedy, A. Multifunctional Nanoparticles for Combining Ultrasonic Tumor Imaging and Targeted Chemotherapy. *J. Natl. Cancer Inst.* **2007**, *99*, 1095–1106.
9. Zhang, Z.; Lee, S.; Gan, C.; Feng, S.-S. Investigation on PLA—TPGS Nanoparticles for Controlled and Sustained Small Molecule Chemotherapy. *Pharm. Res.* **2008**, *25*, 1925–1935.
10. Dong, Y.; Feng, S. S. Poly(D,L-Lactide-Co-Glycolide) (PLGA) Nanoparticles Prepared by High Pressure Homogenization for Paclitaxel Chemotherapy. *Int. J. Pharm.* **2007**, *342*, 208–214.
11. Li, J.; Wang, X.; Wang, C.; Chen, B.; Dai, Y.; Zhang, R.; Song, M.; Lv, G.; Fu, D. The Enhancement Effect of Gold Nanoparticles in Drug Delivery and as Biomarkers of Drug-Resistant Cancer Cells. *ChemMedChem* **2007**, *2*, 374–378.
12. Roeske, J. C.; Nunez, L.; Hoggarth, M.; Labay, E.; Weichselbaum, R. R. Characterization of the Theorectical Radiation Dose Enhancement from Nanoparticles. *Technol. Cancer Res. Treat.* **2007**, *6*, 395–401.
13. O'Neal, D. P.; Hirsch, L. R.; Halas, N. J.; Payne, J. D.; West, J. L. Photo-Thermal Tumor Ablation in Mice Using near Infrared-Absorbing Nanoparticles. *Cancer Lett.* **2004**, *209*, 171–176.
14. El-Sayed, I. H.; Huang, X.; El-Sayed, M. A. Selective Laser Photo-Thermal Therapy of Epithelial Carcinoma Using Anti-EGFR Antibody Conjugated Gold Nanoparticles. *Cancer Lett.* **2006**, *239*, 129–135.
15. Zhang, R. Y.; Wang, X. M.; Wu, C. H.; Song, M.; Li, J. Y.; Lv, G.; Zhou, J.; Chen, C.; Dai, Y. Y.; Gao, F.; *et al*. Synergistic Enhancement Effect of Magnetic Nanoparticles on Anticancer Drug Accumulation in Cancer Cells. *Nanotechnology* **2006**, *17*, 3622–3626.
16. Visaria, R. K.; Griffin, R. J.; Williams, B. W.; Ebbini, E. S.; Paciotti, G. F.; Song, C. W.; Bischof, J. C. Enhancement of Tumor Thermal Therapy Using Gold Nanoparticle-Assisted Tumor Necrosis Factor-Alpha Delivery. *Mol. Cancer Ther.* **2006**, *5*, 1014–1020.
17. Liu, C. J.; Wang, C. H.; Chien, C. C.; Yang, T. Y.; Chen, S. T.; Leng, W. H.; Lee, C. F.; Lee, K. H.; Hwu, Y.; Lee, Y. C.; *et al*. Enhanced X-Ray Irradiation-Induced Cancer Cell Damage by Gold Nanoparticles Treated by a New Synthesis Method of Polyethylene Glycol Modification. *Nanotechnology* **2008**, *19*, 295104.
18. Kong, T.; Zeng, J.; Wang, X. P.; Yang, X. Y.; Yang, J.; McQuarrie, S.; McEwan, A.; Roa, W.; Chen, J.; Xing, J. Z. Enhancement of Radiation Cytotoxicity in Breast-Cancer Cells by Localized Attachment of Gold Nanoparticles. *Small* **2008**, *4*, 1537–1543.
19. Wang, S. Z.; Gao, R. M.; Zhou, F. M.; Selke, M. Nanomaterials and Singlet Oxygen Photosensitizers: Potential Applications in Photodynamic Therapy. *J. Mater. Chem.* **2004**, *14*, 487–493.
20. Takahashi, J.; Misawa, M. Analysis of Potential Radiosensitizing Materials for X-Ray-Induced Photodynamic Therapy. *NanoBiotechnology* **2007**, *3*, 116–126.
21. Morgan, N. Y.; Kramer-Marek, G.; Smith, P. D.; Camphausen, K.; Capala, J. Nanoscintillator Conjugates as Photodynamic Therapy-Based Radiosensitizers: Calculation of Required Physical Parameters. *Radiat. Res.* **2009**, *171*, 236–244.
22. Chatterjee, D. K.; Fong, L. S.; Zhang, Y. Nanoparticles in Photodynamic Therapy: An Emerging Paradigm. *Adv. Drug Delivery Rev.* **2008**, *60*, 1627–1637.
23. Liu, Y. F.; Chen, W.; Wang, S. P.; Joly, A. G. Investigation of Water-Soluble X-Ray Luminescence Nanoparticles for Photodynamic Activation. *Appl. Phys. Lett.* **2008**, *92*, 043901.
24. Chen, W.; Zhang, J. Using Nanoparticles to Enable Simultaneous Radiation and Photodynamic Therapies for Cancer Treatment. *J. Nanosci. Nanotechnol.* **2006**, *6*, 1159–1166.
25. Juzenas, P.; Chen, W.; Sun, Y. P.; Coelho, M. A. N.; Generalov, R.; Generalova, N.; Christensen, I. L. Quantum Dots and Nanoparticles for Photodynamic and Radiation Therapies of Cancer. *Adv. Drug Delivery Rev.* **2008**, *60*, 1600–1614.
26. Lovell, J. F.; Liu, T. W. B.; Chen, J.; Zheng, G. Activatable Photosensitizers for Imaging and Therapy. *Chem. Rev.* **2010**, *110*, 2839–2857.
27. Wang, L.; Yang, W. S.; Read, P.; Larner, J.; Sheng, K. Tumor Cell Apoptosis Induced by Nanoparticle Conjugate in Combination with Radiation Therapy. *Nanotechnology* **2010**, *21*, 475103.
28. Quintiliani, M. Modification of Radiation Sensitivity: The Oxygen Effect. *Int. J. Radiat. Oncol. Biol. Phys.* **1979**, *5*, 1069–1076.
29. Henderson, B. W.; Fingar, V. H. Relationship of Tumor Hypoxia and Response to Photodynamic Therapy Treatment in an Experimental Mouse-Tumor. *Cancer Res.* **1987**, *47*, 3110–3114.
30. Chaplin, D. J.; Durand, R. E.; Olive, P. L. Acute Hypoxia in Tumors: Implications for Modifiers of Radiation Effects. *Int. J. Radiat. Oncol. Biol. Phys.* **1986**, *12*, 1279–1282.
31. Huang, Z.; Chen, Q.; Shakil, A.; Chen, H.; Beckers, J.; Shapiro, H.; Hetzel, F. W. Hyperoxygenation Enhances the Tumor Cell Killing of Photofrin-Mediated Photodynamic Therapy. *Photochem. Photobiol.* **2003**, *78*, 496–502.
32. Gasparro, F. P.; Felli, A.; Schmitt, I. M. Psoralen Photobiology: The Relationship between DNA Damage, Chromatin Structure, Transcription, and Immunogenic Effects. *Recent Results Cancer Res.* **1997**, *143*, 101–127.
33. Malane, M. S.; Gasparro, F. P. T Cell Molecular Targets for Psoralens. *Ann. N.Y. Acad. Sci.* **1991**, *636*, 196–208.

34. Bethea, D.; Fullmer, B.; Syed, S.; Seltzer, G.; Tiano, J.; Rischko, C.; Gillespie, L.; Brown, D.; Gasparro, F. P. Psoralen Photobiology and Photochemotherapy: 50 Years of Science and Medicine. *J. Dermatol. Sci.* **1999**, *19*, 78–88.
35. Shah, K. S.; Glodo, J.; Higgins, W.; Loef, E. V. D. v.; Moses, W. W.; Derenzo, S. E.; Weber, M. J. CeBr3 Scintillators for Gamma-Ray Spectroscopy. *IEEE Trans. Nucl. Sci.* **2005**, *52*, 3157–3159.
36. Loef, E. V. D. v.; Dorenbos, P.; Kramer, K.; Gudel, H. U. Scintillation Properties of $LaCl_3$: Ce^{3+} Crystals: Fast, Efficient, and High-Energy Resolution Scintillators. *IEEE Trans. Nucl. Sci.* **2001**, *48*, 341–345.
37. Dorenbos, P.; Bougrine, E.; deHaas, J. T. M.; vanEijk, C. W. E.; Korzhik, M. V. Scintillation Properties of $GdAlO_3$:Ce Crystals. *Radiat. Eff. Defects Solids* **1995**, *135*, 819–821.
38. Roy, U. N.; Groza, M.; Cui, Y.; Burger, A.; Cherepy, N.; Friedrich, S.; Payne, S. A. A New Scintillator Material. *Nucl. Instrum. Methods Phys. Res., Sect. A* **2007**, *579*, 46–49.
39. Loef, E. V. D. v.; Dorenbos, P.; Eijk, C. W. E. v.; Kramer, K. W.; Gudel, H. U. Scintillation Properties of K_2LaX_5: Ce^{3+} (X = Cl, Br, I). *Nucl. Instrum. Methods Phys. Res., Sect. A* **2005**, *537*, 232–236.
40. Spijker, J. C. v. t.; Dorenbos, P.; Eijk, C. W. E. v.; Kramer, K.; Gudel, H. U. Scintillation and Luminescence Properties of Ce^{3+} Doped K_2LaCl_5. *J. Lumin.* **1999**, *85*, 1–10.
41. Vantspijker, J. C.; Dorenbos, P.; Dehaas, J. T. M.; Vaneijk, C. W. E.; Gudel, H. U.; Kramer, K. Scintillation Properties of K_2LaCl_5 with Ce Doping. *Radiat. Meas.* **1995**, *24*, 379–381.
42. Yuan, J.-L.; Zhang, H.; Chen, H.-H.; Yang, X.-X.; Zhao, J.-T.; Gu, M. Synthesis, Structure and X-Ray Excited Luminescence of Ce^{3+}-Doped AREP2O7-Type Alkali Rare Earth Diphospates (a = Na, K, Pb, Cs; Re = Y, Lu). *J. Solid State Chem.* **2007**, *180*, 3381–3387.
43. Loef, E. V. D. v.; Dorenbos, P.; Eijk, C. W. E. v.; Kramer, K. W.; Gudel, H. U. Scintillation Properties of $LaBr_3$: Ce^{3+} Crystals: Fast, Efficient and High-Energy-Resolution Scintillators. *Nucl. Instrum. Methods Phys. Res., Sect. A* **2002**, *486*, 254–258.
44. Menge, P. R.; Gautier, G.; Iltis, A.; Rozsa, C.; Solovyev, V. Performance of Large Lanthanum Bromide Scintillators. *Nucl. Instrum. Methods Phys. Res., Sect. A* **2007**, *579*, 6–10.
45. Haas, J. T. M. d.; Dorenbos, P. Advances in Yield Calibration of Scintillators. *IEEE Trans. Nucl. Sci.* **2008**, *55*, 1086–1092.
46. Salacka, J. S.; Bacrania, M. K. A Comprehensive Technique for Determining the Intrinsic Light Yield of Scintillators. *IEEE Trans. Nucl. Sci.* **2010**, *57*, 901–909.
47. Moszynski, M.; Wolski, D.; Ludziejewski, T.; Kapusta, M.; Lempicki, A.; Brecher, C.; Wisniewski, D.; Wojtowicz, A. J. Properties of the New LuAP:Ce Scintillator. *Nucl. Instrum. Methods Phys. Res., Sect. A* **1997**, *385*, 123–131.
48. Moses, W. W.; Derenzo, S. E.; Fyodorov, A.; Korzhik, M.; Gektin, A.; Minkov, B.; Aslanov, V. $LuAlO_3$-Ce - a High-Density, High-Speed Scintillator for Gamma-Detection. *IEEE Trans. Nucl. Sci.* **1995**, *42*, 275–279.
49. Moszynski, M.; Kapusta, M.; Mayhugh, M.; Wolski, D.; Flyckt, S. O. Absolute Light Output of Scintillators. *IEEE Trans. Nucl. Sci.* **1997**, *44*, 1052–1061.
50. Lempicki, A.; Randles, M. H.; Wisniewski, D.; Balcerzyk, M.; Brecher, C.; Wojtowicz, A. J. $LuAlO_3$-Ce and Other Aluminate Scintillators. *IEEE Trans. Nucl. Sci.* **1995**, *42*, 280–284.
51. Lempicki, A.; Berman, E.; Wojtowicz, A. J.; Balcerzyk, M.; Boatner, L. A. Cerium-Doped Orthophosphates - New Promising Scintillators. *IEEE Trans. Nucl. Sci.* **1993**, *40*, 384–387.
52. Moses, W. W.; Derenzo, S. E.; Shlichta, P. J. Scintillation Properties of Lead Sulfate. *IEEE Trans. Nucl. Sci.* **1992**, *39*, 1190–1194.
53. Zadneprovski, B. I.; Kamenskikh, I. A.; Kolobanov, V. N.; Mikhailin, V. V.; Shpinkov, I. N.; Kirm, M. Gel Growth, Luminescence, and Scintillation of $PbSO_4$ Crystals. *Inorg. Mater.* **2004**, *40*, 735–739.
54. Zhang, J. G.; Lund, J. C.; Cirignano, L.; Shah, K. S.; Squillante, M. R.; Moses, W. W. Lead Sulfate Scintillator Crystal Growth for PET Applications. *IEEE Trans. Nucl. Sci.* **1994**, *41*, 669–674.
55. Birowosuto, M. D.; Dorenbos, P.; Eijk, C. W. E. v.; Kramer, K. W.; Gudel, H. U. $PrBr_3$: Ce^{3+}: A New Fast Lanthanide Trihalide Scintillator. *IEEE Trans. Nucl. Sci.* **2006**, *53*, 3028–3030.
56. Ogorodnikov, I. N.; Kruzhalov, A. V.; Ivanov, V. Y. Mechanisms of Fast UV-Scintillations in Oxide Crystals with Self-Trapped Excitons. In *Inorganic Scintillators and Their Applications*; Delft University Press (SCINT95): Amsterdam, The Netherlands, 1996; pp 216−219.
57. Baryshevsky, V. G.; Korzhik, M. V.; Moroz, V. I.; Pavlenko, V. B.; Fyodorov, A. A.; Smirnova, S. A.; Egorycheva, O. A.; Kachanov, V. A. YAlO3 - Ce-Fast-Acting Scintillators for Detection of Ionizing-Radiation. *Nucl. Instrum. Methods Phys. Res., Sect. B* **1991**, *58*, 291–293.
58. Mares, J. A.; Beitlerova, A.; Nikl, M.; Solovieva, N.; D'Ambrosio, C.; Blazek, K.; Maly, P.; Nejezchleb, K.; Notaristefani, F. d. Scintillation Response of Ce-Doped or Intrinsic Scintillating Crystals in the Range up to 1 MeV. *Radiat. Meas.* **2004**, *38*, 353–357.
59. de Haas, J. T. M.; Dorenbos, P.; van Eijk, C. W. E. Measuring the Absolute Light Yield of Scintillators. *Nucl. Instrum. Methods Phys. Res., Sect. A* **2005**, *537*, 97–100.
60. Zako, T.; Nagata, H.; Terada, N.; Sakono, M.; Soga, K.; Maeda, M. Improvement of Dispersion Stability and Characterization of Upconversion Nanophosphors Covalently Modified with PEG as a Fluorescence Bioimaging Probe. *J. Mater. Sci.* **2008**, *43*, 5325–5330.
61. Vetrone, F.; Boyer, J. C.; Capobianco, J. A.; Speghini, A.; Bettinelli, M. A Spectroscopic Investigation of Trivalent Lanthanide Doped Y_2O_3 Nanocrystals. *Nanotechnology* **2004**, *15*, 75–81.
62. Chen, W.; Zhang, J.; Westcott, S. L.; Joly, A. G.; Malm, J. O.; Bovin, J. O. The Origin of X-Ray Luminescence from CdTe Nanoparticles in CdTe/BaFBr: Eu^{2+} Nanocomposite Phosphors. *J. Appl. Phys.* **2006**, *99*, 034302.
63. Liu, Y. F.; Chen, W.; Wang, S. P.; Joly, A. G.; Westcott, S.; Woo, B. K. X-Ray Luminescence of LaF_3: Tb^{3+} and LaF_3: Ce^{3+}, Tb^{3+} Water-Soluble Nanoparticles. *J. Appl. Phys.* **2008**, *103*, 063105–063105-7.
64. Zhang, H. P.; Lu, M. K.; Xiu, Z. L.; Zhou, G. J.; Wang, S. F.; Zhou, Y. Y.; Wang, S. M. Influence of Processing Conditions on the Luminescence of YVO4: Eu^{3+} Nanoparticles. *Mater. Sci. Eng. B* **2006**, *130*, 151–157.
65. Wisniewski, D.; Wojtowicz, A. J.; Lempicki, A. Spectroscopy and Scintillation Mechanism in $LuAlO_3$:Ce. *J. Lumin.* **1997**, *72−74*, 789–791.
66. Wojtowicz, A. J.; Szupryczynski, P.; Wisniewski, D.; Glodo, J.; Drozdowski, W. Electron Traps and Scintillation Mechanism in $LuAlO_3$:Ce. *J. Phys.: Condens. Matter* **2001**, *13*, 9599–9619.
67. Dorenbos, P. Scintillation Mechanisms in Ce^{3+} Doped Halide Scintillators. *Phys. Status Solidi A* **2005**, *202*, 195–200.
68. Gregas, M. K.; Scaffidi, J. P.; Lauly, B.; Vo-Dinh, T. Surface-Enhanced Raman Scattering Detection and Tracking of Nanoprobes: Enhanced Uptake and Nuclear Targeting in Single Cells. *Appl. Spectrosc.* **2010**, *64*, 858–866.
69. Fawell, S.; Seery, J.; Daikh, Y.; Moore, C.; Chen, L. L.; Pepinsky, B.; Barsoum, J. Tat-Mediated Delivery of Heterologous Proteins into Cells. *Proc. Natl. Acad. Sci. U. S. A.* **1994**, *91*, 664–8.
70. Brooks, H.; Lebleu, B.; Vives, E. Tat Peptide-Mediated Cellular Delivery: Back to Basics. *Adv. Drug Delivery Rev.* **2005**, *57*, 559–577.
71. Zorko, M.; Langel, U. Cell-Penetrating Peptides: Mechanism and Kinetics of Cargo Delivery. *Adv. Drug Delivery Rev.* **2005**, *57*, 529–545.
72. Reis, P. A.; Valente, L. M. P.; Almeida, C. M. R. A Fast and Simple Methodology for Determination of Yttrium as an Inert Marker in Digestibility Studies. *Food Chem.* **2008**, *108*, 1094–1098.
73. Schubert, D.; Dargusch, R.; Raitano, J.; Chan, S. W. Cerium and Yttrium Oxide Nanoparticles Are Neuroprotective. *Biochem. Biophys. Res. Commun.* **2006**, *342*, 86–91.
74. Torchilin, V. P.; Levchenko, T. S.; Rammohan, R.; Volodina, N.; Papahadjopoulos-Sternberg, B.; D'Souza, G. G. M. Cell

Transfection *in Vitro* and *in Vivo* with Nontoxic Tat Peptide-Liposome-DNA Complexes. *Proc. Natl. Acad. Sci. U. S. A.* **2003**, *100*, 1972–1977.
75. Manickam, D. S.; Bisht, H. S.; Wan, L.; Mao, G. Z.; Oupicky, D. Influence of Tat-Peptide Polymerization on Properties and Transfection Activity of Tat/DNA Polyplexes. *J. Controlled Release* **2005**, *102*, 293–306.
76. Kim, K.; Han, J.; Kim, H.; Lee, M. Expression, Purification and Characterization of Tat-High Mobility Group Box-1a Peptide as a Carrier of Nucleic Acids. *Biotechnol. Lett.* **2008**, *30*, 1331–1337.
77. Weisenthal, L. M.; Dill, P. L.; Kurnick, N. B.; Lippman, M. E. Comparison of Dye Exclusion Assays with a Clonogenic-Assay in the Determination of Drug-Induced Cyto-Toxicity. *Cancer Res.* **1983**, *43*, 258–264.
78. Plumb, J. A. Ch. 2-Cell Sensitivity Assays/Clonogenic Assay. In *Cytotoxic Drug Resistance Mechanisms*; Brown, R.; Boger-Brown, U., Eds.; Humana Press: Totowa, NJ, 1999; pp 25−30.
79. Franken, N. A. P.; Rodermond, H. M.; Stap, J.; Haveman, J.; van Bree, C. Clonogenic Assay of Cells *in Vitro*. *Nat. Protoc.* **2006**, *1*, 2315–2319.
80. Mueller, H.; Kassack, M. U.; Wiese, M. Comparison of the Usefulness of the MTT, ATP, and Calcein Assays to Predict the Potency of Cytotoxic Agents in Various Human Cancer Cell Lines. *J. Biomol. Screen.* **2004**, *9*, 506–515.
81. Gorodetsky, R.; Mou, X.; Pfeffer, M. R.; Peretz, T.; Levy-Agababa, F.; Vexler, A. M. Sub-Additive Effect of the Combination of Radiation and Cisplatin in Cultured Murine and Human Cell Lines. *Isr. J. Med. Sci.* **1995**, *31*, 95–100.
82. Felice, D. L.; Sun, J.; Liu, R. H. A Modified Methylene Blue Assay for Accurate Cell Counting. *J. Funct. Foods* **2009**, *1*, 109–118.
83. Oliver, M. H.; Harrison, N. K.; Bishop, J. E.; Cole, P. J.; Laurent, G. J. A Rapid and Convenient Assay for Counting Cells Cultured in Microwell Plates Application for Assessment of Growth Factors. *J. Cell Sci.* **1989**, *92*, 513–518.
84. Pelletier, B.; Dhainaut, F.; Pauly, A.; Zahnd, J. P. Evaluation of Growth Rate in Adhering Cell Cultures Using a Simple Colorimetric Method. *J. Biochem. Biophys. Methods* **1988**, *16*, 63–73.
85. Dent, M. F.; Hubbold, L.; Radford, H.; Wilson, A. P. The Methylene Blue Colorimetric Microassay for Determining Cell Line Response to Growth Factors. *Cytotechnology* **1995**, *17*, 27–33.
86. Scragg, M. A.; Ferreira, L. R. Evaluation of Different Staining Procedures for the Quantification of Fibroblasts Cultured in 96-Well Plates. *Anal. Biochem.* **1991**, *198*, 80–85.
87. Chithrani, D. B.; Jelveh, S.; Jalali, F.; van Prooijen, M.; Allen, C.; Bristow, R. G.; Hill, R. P.; Jaffray, D. A. Gold Nanoparticles as Radiation Sensitizers in Cancer Therapy. *Radiat. Res.* **2010**, *173*, 719–728.
88. Chiu, S. J.; Lee, M. Y.; Chou, W. G.; Lin, L. Y. Germanium Oxide Enhances the Radiosensitivity of Cells. *Radiat. Res.* **2003**, *159*, 391–400.
89. Hainfeld, J. F.; Slatkin, D. N.; Smilowitz, H. M. The Use of Gold Nanoparticles to Enhance Radiotherapy in Mice. *Phys. Med. Biol.* **2004**, *49*, N309–N315.
90. Hainfeld, J. F.; Dilmanian, F. A.; Zhong, Z.; Slatkin, D. N.; Kalef-Ezra, J. A.; Smilowitz, H. M. Gold Nanoparticles Enhance the Radiation Therapy of a Murine Squamous Cell Carcinoma. *Phys. Med. Biol.* **2010**, *55*, 3045–3059.
91. Kim, J. K.; Seo, S. J.; Kim, K. H.; Kim, T. J.; Chung, M. H.; Kim, K. R.; Yang, T. K. Therapeutic Application of Metallic Nanoparticles Combined with Particle-Induced X-Ray Emission Effect. *Nanotechnology* **2010**, *21*, 425102.
92. Chattopadhyay, N.; Cai, Z. L.; Pignol, J. P.; Keller, B.; Lechtman, E.; Bendayan, R.; Reilly, R. M. Design and Characterization of HER-2-Targeted Gold Nanoparticles for Enhanced X-Radiation Treatment of Locally Advanced Breast Cancer. *Mol. Pharmaceutics* **2010**, *7*, 2194–2206.